A Low-Cost Wideband SIW Antenna with Bilateral Slots on FR4 Epoxy for Ku-Band Applications

Dounia Chrij[1], Asma Khabba[1], Zakaria El Ouadi[1], Lahcen Sellak[2], Jamal Amadid[3],
Omaima Benkhadda[4], Saida Ibnyaich[1], Abdelouhab Zeroual[1], and Ahmed J. A. Al-Gburi[5, *]

[1]*I2SP Research Team, Department of Physics, Faculty of Sciences Semlalia, Cadi Ayyad University, Marrakech, Morocco*
[2]*LISAD Research Laboratory, Industrial Engineering Department, National School of Applied Sciences*
Ibn Zohr University, Agadir, Morocco
[3]*ISGA Higher Institute of Engineering & Business, Marrakesh, Morocco*
[4]*Laboratory of Mathematics, Computer Science, Electrical Engineering and Physics (LAMIGEP)*
EMSI-Marrakech, Morocco
[5]*Center for Telecommunication Research & Innovation (CeTRI)*
Fakulti Teknologi dan Kejuruteraan Elektronik dan Komputer (FTKEK)
Universiti Teknikal Malaysia Melaka (UTeM), Melaka 76100, Malaysia

ABSTRACT: This article presents an approach to expanding the impedance bandwidth of a bilateral slotted antenna backed by a substrate-integrated waveguide (SIW) cavity using high-order radiation modes. By trimming a section of the conductive ground plane and connecting one side of the bottom long slot with a via, the three hybrid modes of the cavity are perturbed and merged to achieve a broad bandwidth. The optimized antenna is fed by a microstrip transmission line for Ku-band applications, demonstrating an impressive impedance bandwidth of 6.68 GHz (a fractional bandwidth of 41%) ranging from 12.82 GHz to 19.5 GHz, with a peak gain of 6.6 dBi. Compared to previous studies, the proposed antenna offers not only a wide bandwidth but also a compact size, with dimensions of $29.7 \times 22 \, \text{mm}^2$, and its electrical dimensions are $1.6\lambda_0 \times 1.19\lambda_0$, where λ_0 is the free space wavelength at the center frequency $f_{\text{center}} = 16.16$ GHz. Additionally, it has low production costs due to fabrication on an inexpensive FR4 substrate. The antenna was initially simulated using HFSS software, and to validate the accuracy of the results, it was also analyzed with CST Microwave Studio. Moreover, a prototype was constructed for experimental testing, with measured results showing strong agreement with the simulations.

1. INTRODUCTION

Antenna design is a key aspect of modern communication systems. However, there is a growing demand for low-profile, cost-effective antennas that deliver high-performance radiation characteristics, such as high gain and wide bandwidth, for advanced wireless communication applications. Firstly, Deslandes and Wu [1] introduced a technology known as Substrate Integrated Waveguide (SIW), which offers a low-cost and easily manufacturable solution using PCB (printed-circuit-board) process. It also allows for seamless integration with planar circuits. A SIW structure consists of two lines of conductive cylinders positioned along the outer edges of a dielectric substrate, with electrically conductive metal plates covering the top and bottom surfaces. This configuration provides propagation characteristics similar to conventional metallic waveguides [2]. Later, SIW technique was applied to design and fabricate filters and slot antennas [3, 4]. However, SIW slot antennas typically suffer from limited bandwidth because of the high-quality factor (Q) of SIW cavity [5].

Various solutions have been investigated to overcome the narrow bandwidth limitations of cavity-backed slot antennas. In [6], a shorted via was added above the slot to create an-other resonance, improving the antenna's bandwidth to 2.2%. In [7], dual-resonant slots were employed to create dual resonances, enhancing the antenna's impedance bandwidth to 4% by combining two hybrid modes. In [8], a perturbation method involving two corner cuts along opposite sides of the cavity's diameter increased the impedance bandwidth to 5.7%. In [9], the bandwidth was increased to 24% by eliminating the dielectric substrate beneath the radiating slot. A two-stacked cavity SIW structure was explored in [10], achieving a bandwidth of 150 MHz. However, the techniques proposed in [6–8, 10] require expensive substrate materials, resulting in larger antenna sizes. Various slot shapes have also been incorporated into SIW cavity-backed structures to achieve wideband antennas. In [11], a bow-tie slot was engraved on the top side of the SIW cavity-backed antenna, resulting in a 9.43% impedance bandwidth. In [12], a modified triangular ring slot was used to excite two hybrid modes, achieving an impedance bandwidth improvement of up to 13.89% with moderate gain. In [13], two curved slots etched on the top plane of the SIW antenna and two resonant frequencies were produced at 11.34 GHz and 18.44 GHz, with corresponding fractional bandwidths of 4.409% and 24.29%, respectively.

Recently, several other efforts have been made to enhance bandwidth for Ku band applications. In [14], an offset feed-

* Corresponding author: Ahmed Jamal Abdullah Al-Gburi (ahmedjamal@ieee.org, engahmed_jamall@yahoo.com).

ing technique was applied to an SIW slot antenna, achieving a wideband response at 14.54 GHz with a fractional bandwidth of 19.96%. In [15], an SIW horn antenna was developed, where a partially open conductor section was linked to the feeding structure via a slotted transition, expanding the bandwidth up to 59%. Additionally, a defective ground structure was employed [16], resulting in a bandwidth improvement of up to 23%. While these studies yielded positive results [15, 16], they relied on costly Roger materials and involved complex designs.

This paper aims to present a new perturbation technique using higher-order radiation modes to expand the bandwidth performance of a cavity-backed SIW antenna. The design incorporates bilateral slots as radiating components, fed by a microstrip transmission line. One side of the long slot on the conductive bottom plane is connected to a via, and a section of the ground plane's length is clipped to create a wideband, low-profile antenna. The antenna is cost-effective, as it is fabricated on a low-cost FR4 substrate, and offers moderate gain. The proposed design achieves a broad impedance bandwidth ranging from 12.82 to 19.5 GHz (41%) with $S_{11} \leq -10$ dB, meeting the requirements for Ku band applications.

This paper is organized as follows. Section 2 details the proposed design and its development stages, along with an explanation of the antenna's working mechanism. Section 3 presents a parametric study. Section 4 discusses the results, including measurement results that align well with simulations. Finally, Section 5 concludes the paper.

2. ANTENNA CONFIGURATION AND OPERATING PRINCIPLE

2.1. Proposed Antenna Configuration

Using the HFSS tool, the geometry of the proposed design, shown in Figure 1, is fabricated entirely on a single-layer substrate made of Epoxy FR-4 (with a permittivity of $\varepsilon_r = 4.4$, a loss tangent of $\tan_\delta = 0.02$, and a thickness of $h = 1.6$ mm). A 50 Ω microstrip line feeds the antenna. The choice of the FR4 substrate is motivated by its low cost and easy availability, which aims to achieve a wide impedance bandwidth cost-

effectively. The four sidewalls are formed by aligning via holes in four rows along the antenna's edges, while the upper and lower sides of the cavity are crafted from a copper layer with a modified ground plane. To minimize leakage losses between the via gaps and ensure performance comparable to conventional metallic cavities, careful attention is paid to selecting the diameter of the cylinder (d) and the pitch (p) between neighboring vias. Specifically, the conditions $d/\lambda_0 \leq 0.1$ (where λ_0 is the free-space wavelengths) and $d/p \geq 0.5$ are met to achieve optimal performance [2]. Acting as radiating elements from the SIW cavity to free space, a long slot ($ls_0 \times ws_0$) is engraved on the bottom plane at a distance dsu_0 from the cavity's sidewall, while a short slot ($ls_1 \times ws_1$) is etched on the top wall of the cavity, positioned at a distance dsu_1 from the upper sidewall of the same cavity. It is crucial to recognize that one side of the long slot on the conductive ground plane is connected to a via hole. An offset is introduced between the two slots to achieve a wide bandwidth frequency response, ranging from 12.21 to 17.94 GHz (fractional bandwidth 38%), with $S_{11} \leq -10$ dB, covers the requirement of Ku band application. The predicted dimensions of the SIW cavity can be determined using the operating frequency formula as shown in Equation (1). In this formula, c represents the speed of light in a vacuum, and ε_r denotes the relative dielectric permittivity, while W_{eff}, L_{eff}, and h correspond to the effective width, effective length, and height of the SIW cavity, respectively. The cavity's effective length (L_{eff}) is calculated in Equation (2), and the cavity's effective width (W_{eff}) is determined in Equation (3). In this context, m and n represent the numbers of half-wave fluctuations of the field in the x and y directions, respectively. The overall antenna dimensions are summarized in Table 1.

$$f_r(TE_{mnl}) = \frac{c}{2\sqrt{\varepsilon_r}} \sqrt{\left(\frac{m}{L_{eff}}\right)^2 + \left(\frac{n}{W_{eff}}\right)^2 + \left(\frac{l}{h}\right)^2} \quad (1)$$

$$L_{eff} = L_{cav} - \frac{d^2}{0.95 \times p} \quad (2)$$

$$W_{eff} = W_{cav} - \frac{d^2}{0.95 \times p} \quad (3)$$

TABLE 1. Dimensional parameters for the wideband SIW antenna.

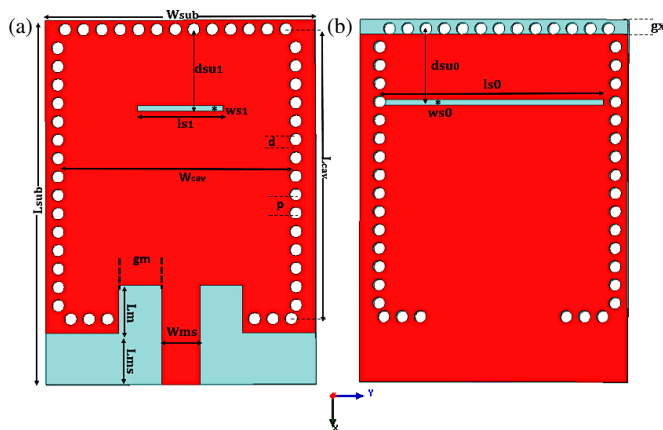| Parameter	Dimension (mm)	Parameter	Dimension (mm)
L_{sub}	29.7	ls_0	18
W_{sub}	22	ls_1	7
L_{cav}	23.6	$ws_1 = ws_0$	0.5
W_{cav}	19.4	dsu_0	5.8
W_{ms}	3.1	dsu_1	6.2
L_{ms}	4.2	d	1
g_m	3.5	p	1.5
L_m	3.9	g_x	1.2

FIGURE 1. Geometry of the suggested wideband antenna at: (a) top view and (b) bottom view.
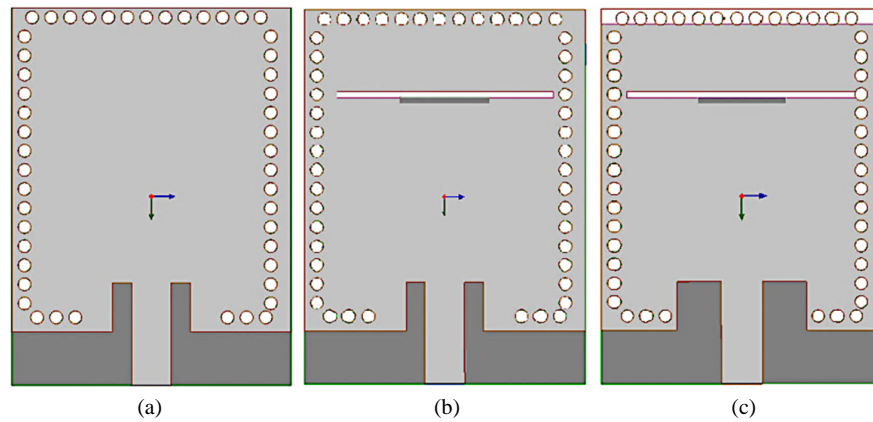
FIGURE 2. Antenna development stages. (a) Only SIW cavity (Stage I). (b) Conventional SIW antenna with bilateral slots (Stage II). (c) Wideband proposed antenna (Stage III).

2.2. Operating Principle

As illustrated in Figure 2, the development of the optimized antenna occurs in three stages. In the first stage, the SIW cavity is created without loading slots with a fall ground plane. The second stage focuses on the conventional SIW antenna, which includes bilateral slots where the long slot is etched at the fall ground plane and the short slot engraved at the top plane. In the final stage, the proposed antenna is formed by integrating one side of the long slot with a via hole and shortening a section of the ground plane's length. To understand the impact of each stage on antenna performance the reflection coefficient (S_{11}) versus frequency is simulated and shown in Figure 3.

FIGURE 3. Reflection coefficient S_{11} (dB) for the three stages.

In Stage I (black curve), the SIW cavity antenna exhibits two resonant frequencies with poor reflection coefficients and narrow passbands. However, in Stage II (blue curve), representing the conventional SIW antenna, a new resonant frequency emerges, and the reflection coefficients improve to better than -15 dB. In Stage III (red curve), corresponding to the proposed antenna, an additional resonant frequency appears, resulting in a wideband response. To explore the operating mechanism of the proposed antenna, the electric field distributions for Stage I, where the two-sided slots are absent from the SIW cavity, are illustrated in Figure 4. The complexity in the electric field distri-

bution within the cavity arises from the superposition of higher-order modes, leading to overlapping. As a result, three hybrid modes are generated. Notably, at 12.44 GHz, there is a mixing of the TE_{310} and TE_{230} modes. At 14.73 GHz, the dominant mode is TE_{330}, with some influence from the higher-order mode TE_{410}. In contrast, the hybrid mode at 17.14 GHz consists of a strong higher mode TE_{430} combined with a weaker higher mode TE_{510}. The real part input impedance of the design configurations is represented in Figure 5. It is evident that the loading of the slots in Stage II significantly affects cavity modes especially the second hybrid mode. Hence, the second resonant frequency at 14.73 GHz occurs. Therefore, in Stage III these higher cavity modes are merged, and then bandwidth is improved. Consequently, the antenna achieves wideband operation and resonates at four main frequencies: $f_1 = 13.75$ GHz, $f_2 = 16$ GHz, $f_3 = 17.47$ GHz, and $f_4 = 18.67$ GHz. The surface current distribution of the suggested design at the three highest operating frequencies is shown in Figure 6. The surface current is primarily focused along the length of the long slot, which accounts for the highest frequencies. Additionally, there is a notable accumulation at the edge of the feed line and the upper edge of the ground plane, while a minimal amount of current is present along the short slot at frequencies f_2 and f_4. However, the maximum current distribution occurs along the short slot at frequency f_3, indicating that this resonant frequency is strongly influenced by this slot.

2.3. Parametric Study

To achieve the result of a wideband antenna, an intensive parametric investigation was carried out. Initially, as shown in Figure 7, multiple parameter studies were conducted simultaneously to assess the effect of various design parameters on antenna performance. It is noted that the only values of $g_m = 3.5$, $g_x = 1.2$, and $ls_0 = 18$ offer a wide impedance bandwidth extending from 12.86 to 19.05 GHz (38.62%) with $S_{11} \leq -10$ dB. Another set of individual parametric studies is conducted to analyze how each parameter influences the band response characteristics. From Figure 8, where the aperture g_m varies from 1.5 mm to 3.5 mm, the antenna transitions from a
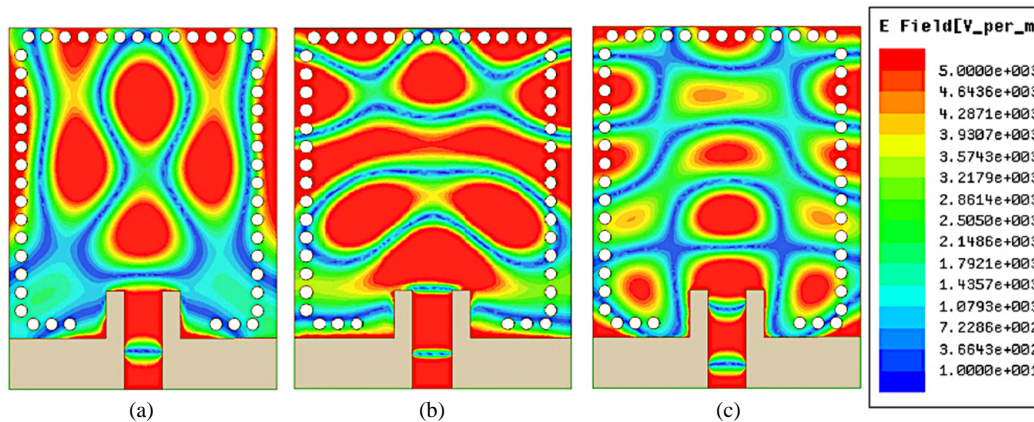
FIGURE 4. Distributions of the electric field inside the SIW-cavity only (a) at 12.44 GHz; (b) at 14.73 GHz; (c) at 17.14 GHz.
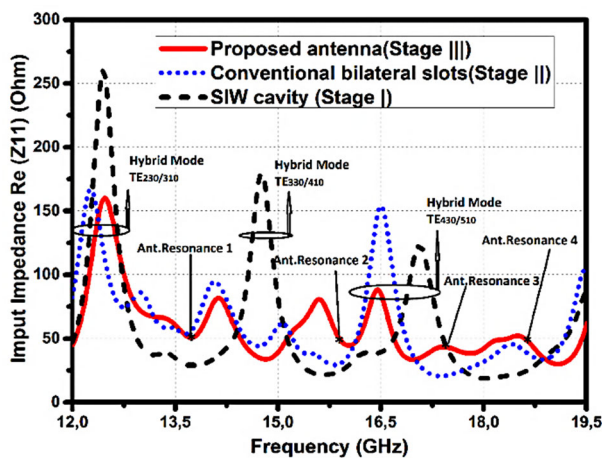

FIGURE 5. Real input impedance (Z_{11}) curves for the SIW cavity alone (Stage I), with bilateral slots (Stage II), and for the proposed antenna (Stage III).

dual-band to a wideband response with a slight shift in the second resonant frequency f_2. Moreover, Figure 9 demonstrates that the maximum bandwidth can be achieved with improved impedance matching at an optimal value of $g_x = 1.2$ mm.

From Figure 10, it can be seen that as the length parameter of the long slot ls_0 decreases from 18 mm to 16.8 mm, the third resonant frequency f_3 becomes unstable, while the higher resonant frequency f_4 shifts upward from 17.47 GHz to 18 GHz. The frequency f_1 remains unchanged at 13.75 GHz. Therefore, the optimal value for ls_0 is determined to be 18 mm, at which point the antenna responds from narrow dual-band to wideband. However, lengths greater than 18 mm and up to 19.8 mm are not considered, as they fall within the via hole. Additionally, the impact of the long slot width is illustrated in Figure 11, and the width ws_0 does not affect the lower resonant frequency f_1; however, the two upper resonant frequencies (f_3, f_4) are modified, significantly affecting the impedance bandwidth.

The optimal value for maintaining a wide bandwidth is found to be 0.5 mm. Conversely, as shown in Figure 12 increasing the position dsu_0 of the long slot from the upper side wall of the cavity results in bandwidth distortion and changes in f_2 and f_4. Therefore, the optimal value of dsu_0 is determined to be

5.8 mm, which provides a wide bandwidth. Similarly, in Figure 13, changing the length of the short slot ls_1 affects all four resonant frequencies. As ls_1 increases, the impedance bandwidth improves, but it becomes perturbed beyond the optimal value of 7 mm.

Additionally, Figure 14 shows that when the width ws_1 of the short slot is altered, the lower resonant frequencies f_1 and f_2 remain nearly constant, while the two higher resonant frequencies f_3 and f_4 are affected. Simultaneously, as shown in Figure 15, decreasing the position dsu_1 of the long slot from the top side wall of the cavity significantly affects the antenna's return loss at all resonant frequencies. The impedance bandwidth experiences slight distortion, leading to the conclusion that the optimal value for dsu_1 is 5.8 mm.

3. RESULTS AND DISCUSSION

All analyses of the suggested antenna were conducted using HFSS ANSYS software. To verify the accuracy of the results, additional simulations were performed using CST Microwave Studio. As shown in Figure 16, it can be demonstrated that the antenna maintains the same operating band between 12.85 GHz and 19.1 GHz, with only slight variations in the S_{11} values at resonant frequencies f_2 and f_4. This difference can be attributed to the use of the Finite Element Method (FEM) in HFSS and the Finite Integration Technique (FIT) in CST. Furthermore, to confirm the simulated results of the suggested design, a prototype antenna was constructed using an epoxy FR4 substrate with a standard thickness of 1.6 mm and a dielectric constant of 4.4. Photographs of the top and bottom views of the prototype are presented in Figure 17. The reflection coefficient of the fabricated antenna was measured using a 3656D Vector Network Analyzer with a frequency range extending up to 20 GHz. As depicted in Figure 18, the measured fractional bandwidth (for S_{11} below -10 dB) is 41%, ranging from 12.82 GHz to 19.5 GHz, which is close to the simulated fractional bandwidth of 38.6%, spanning from 12.85 GHz to 19.05 GHz. This meets the requirements for Ku band applications, with some variations at the resonant frequencies. A new resonant frequency appears at 15.24 GHz, and the resonant frequency f_2 shifts upward from 16 GHz to 16.77 GHz. Several
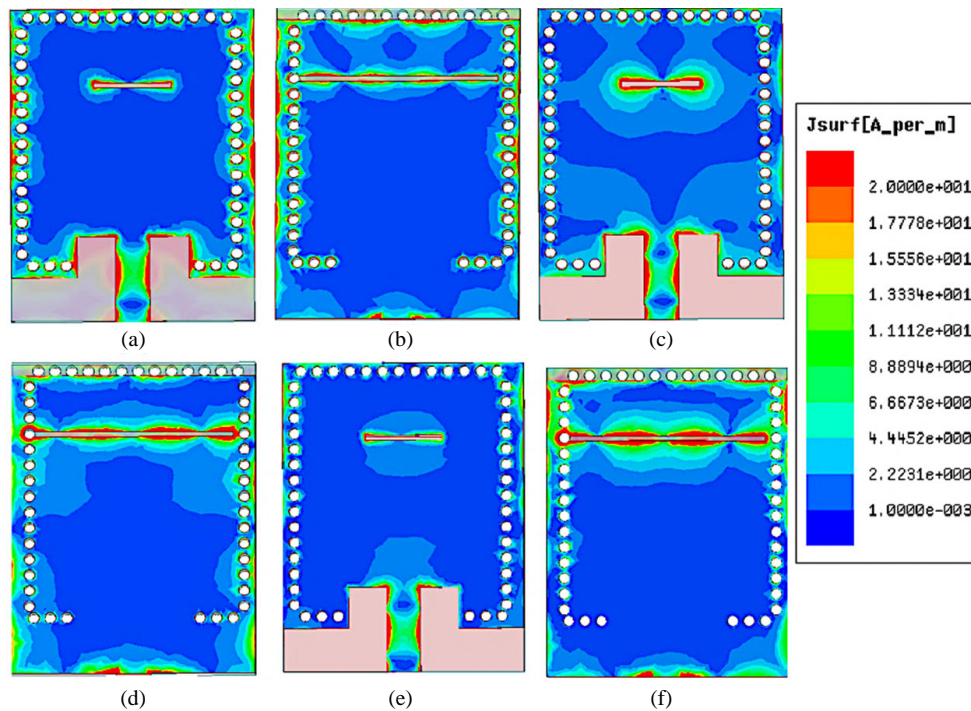
FIGURE 6. The current distribution of the proposed structure at the three highest resonances in the top and bottom surfaces. (a), (b) at $f_2 = 16$ GHz, (c), (d) at $f_3 = 17.47$ GHz, (e), (f) at $f_4 = 18.67$ GHz.
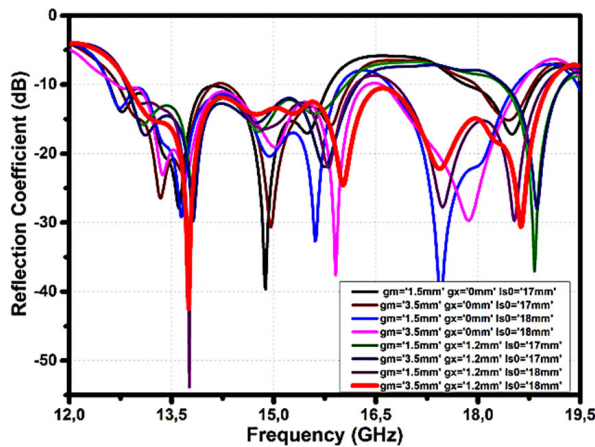

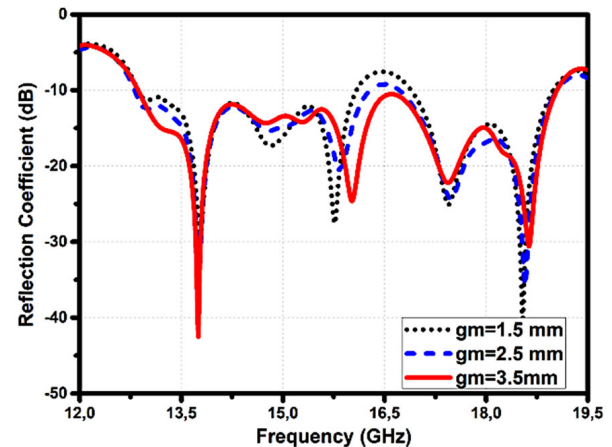**FIGURE 7**. Simultaneous parametric study.

FIGURE 8. Changes in reflection coefficient by varying the aperture g_m.

factors contribute to these discrepancies, including the effects of the soldered SMA connector, RF cables, fabrication imperfections, and the measurement environment. Likewise, the simulated and experimental Voltage Standing Wave Ratio (VSWR) results confirm proper antenna matching, with a VSWR value below 2 across the operating band, as seen in Figure 19. Similarly, Figure 20 illustrates that the simulated and experimental reflection coefficient phases remain at 0 across all resonant frequencies, indicating good impedance matching.

As part of additional efforts to enhance the accuracy of the simulated results, the SMA connector was incorporated into the antenna simulations. Figure 21 presents a comparison of the simulated reflection coefficient S_{11} with and without the inclusion of the SMA connector, alongside the measured results. As

seen in the figure, the simulated results that include the SMA connector align more closely with the measured data, highlighting the significance of incorporating the connector in the simulation model. The simulation without the SMA connector (red solid line) shows a slight deviation from the measured results (blue dashed line) in terms of resonance frequencies and reflection coefficient value. In contrast, the simulation with the SMA connector (green dotted line) demonstrates a much better agreement with the measured curve, particularly in terms of the S_{11} value and location of resonance frequencies. Although there are minor differences between the measured and simulated results (even with the SMA connector), they can be attributed to fabrication imperfections, material property variations, and measurement uncertainties.
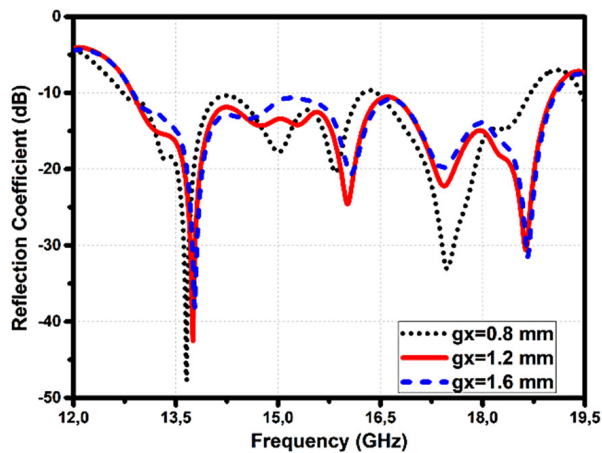
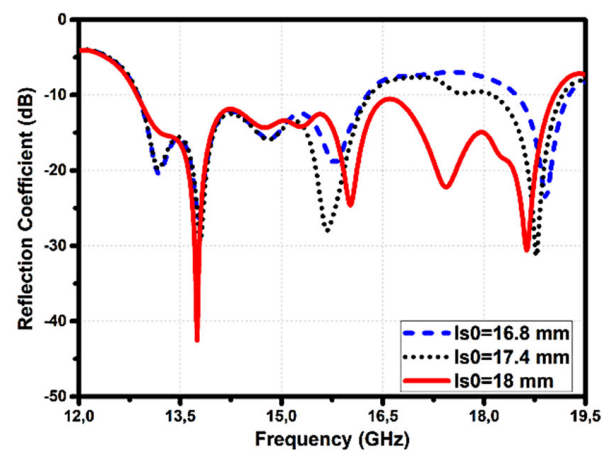FIGURE 9. Change in reflection coefficient by varying the portion g_x.

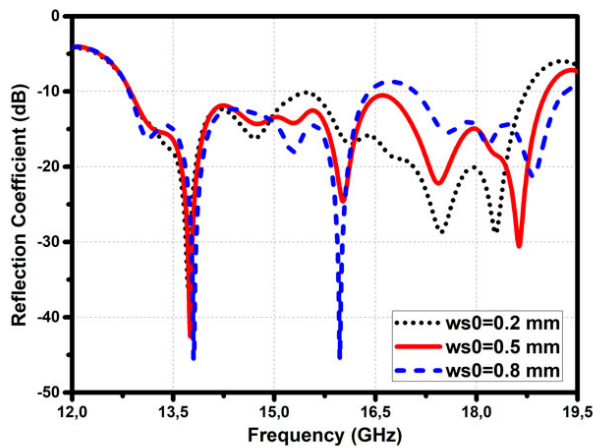FIGURE 10. Changes in reflection coefficient by varying long slot length ls_0.

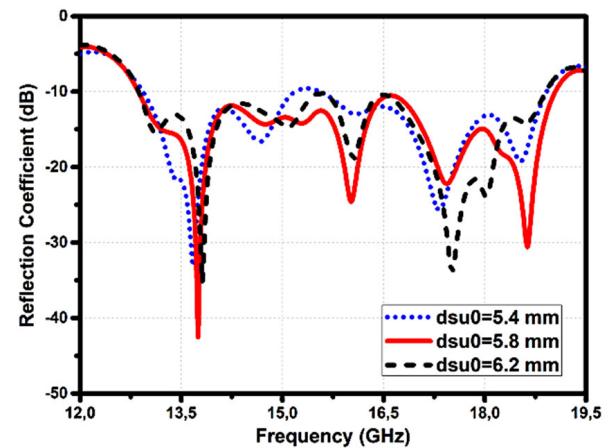FIGURE 11. Changes in reflection coefficient by varying long slot width ws_0.

FIGURE 12. Changes in reflection coefficient by varying long slot position dsu_0.
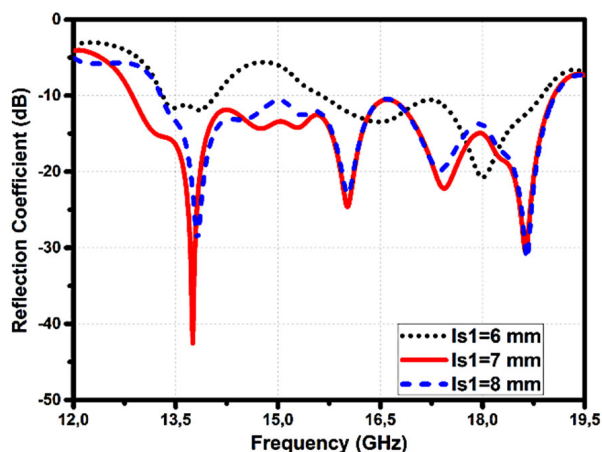

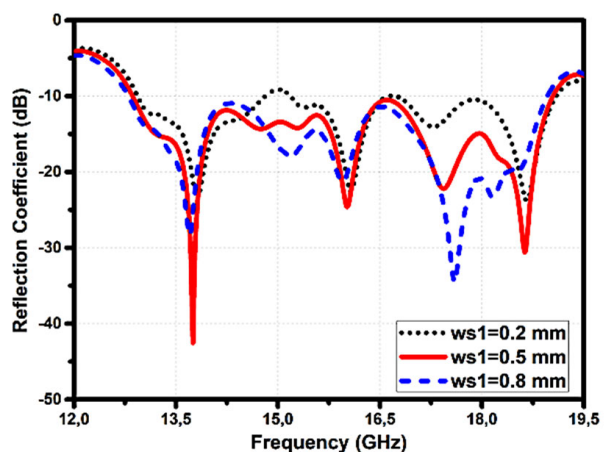FIGURE 13. Changes in reflection coefficient by varying short slot length ls_1.

FIGURE 14. Changes in reflection coefficient by varying short slot width ws_1.

The total gain radiation performance of the proposed antenna has been simulated using HFSS, with the CST-simulated pattern also included for comparison in Figure 22. The results from the two simulations show good agreement. The normalized far-field pattern was analyzed in two cut-planes, the XZ-plane ($\phi = 0°$) and the YZ-plane ($\phi = 90°$), at four main resonance
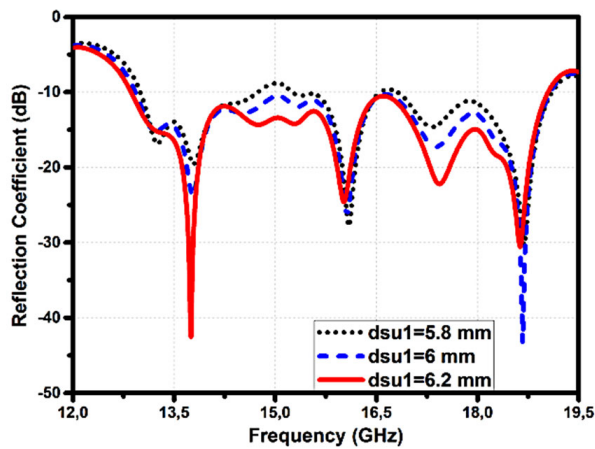
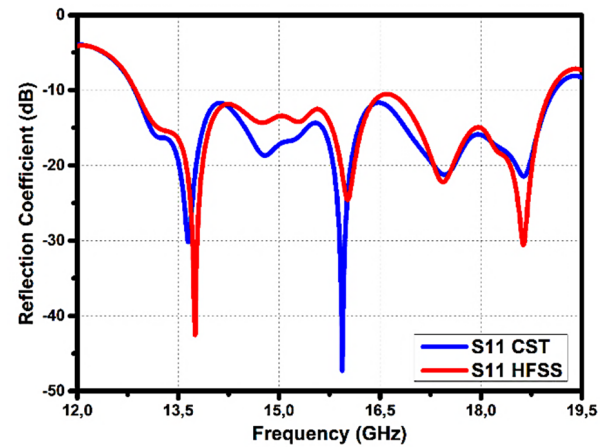FIGURE 15. Changes in reflection coefficient by varying short slot position dsu_1.

FIGURE 16. Comparison of simulated reflection coefficient (S_{11}) using CST and HFSS.
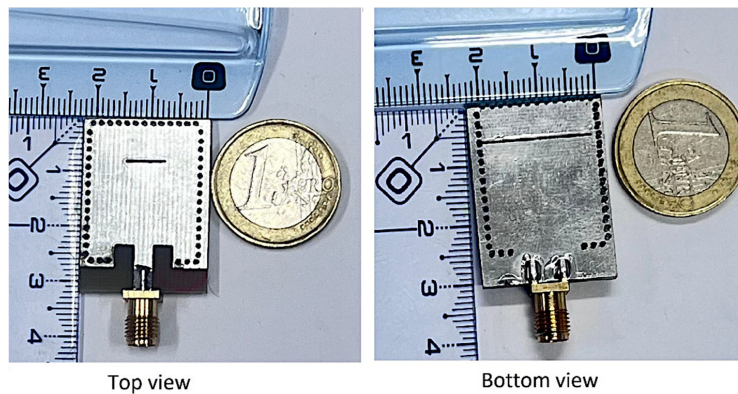

Top view   Bottom view

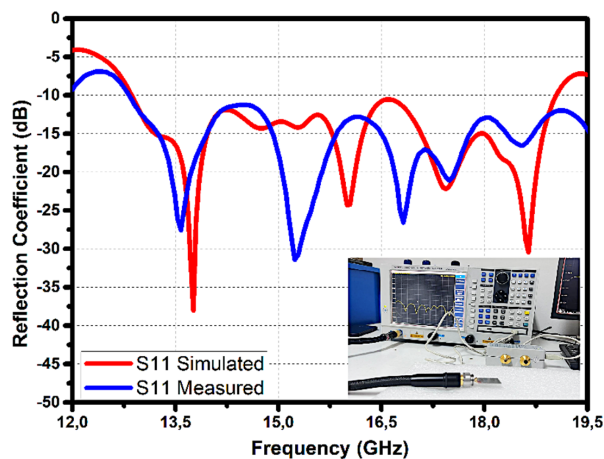FIGURE 17. Photographs of the fabricated antenna.

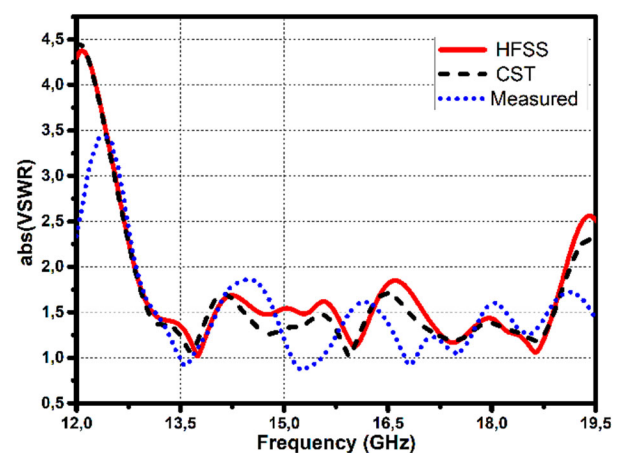FIGURE 18. Comparison of simulated and measured reflection coefficients (S_{11}).

FIGURE 19. Comparison of simulated and measured VSWRs.

frequencies: 13.75 GHz, 16 GHz, 17.47 GHz, and 18.67 GHz. The proposed antenna exhibits a unidirectional pattern in the broadside direction at 13.75 GHz, a good omnidirectional pattern at 16 GHz, a semi-omnidirectional pattern at 17.47 GHz, and a bidirectional pattern at the higher resonant frequency of 18.67 GHz.

For further analysis, the simulated gain and radiation efficiency of the wideband antenna were examined using HFSS and CST software. As shown in Figure 23(a)), the simulated maximum gain across the operating frequency range varies between 2.83 and 6.6 dBi, which is considered reasonable compared to similar studies in the literature. The relatively modest gain is attributed to the antenna's omnidirectional radiation
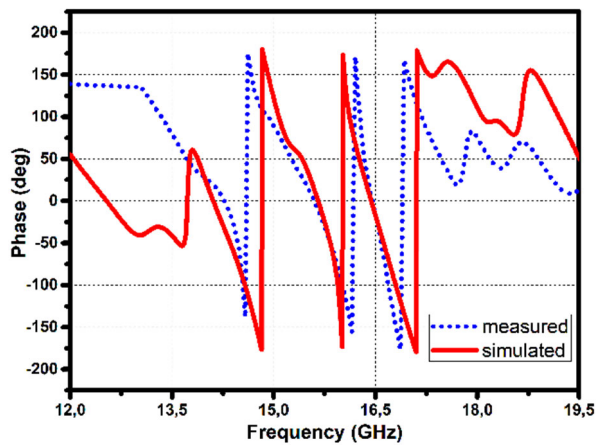
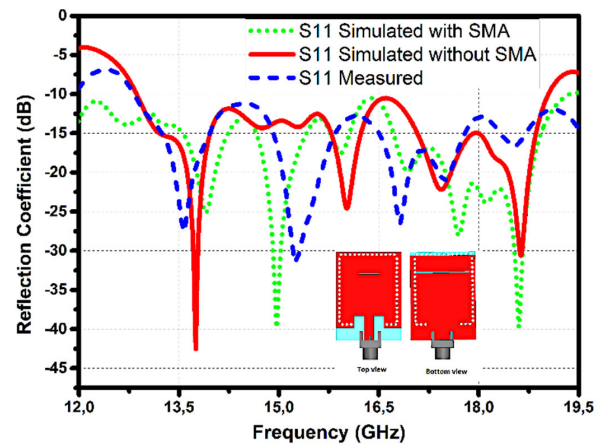FIGURE 20. Comparison of simulated and measured phases.

FIGURE 21. Comparison of reflection coefficients (S_{11}) for simulated results with and without SMA connector and measured results.
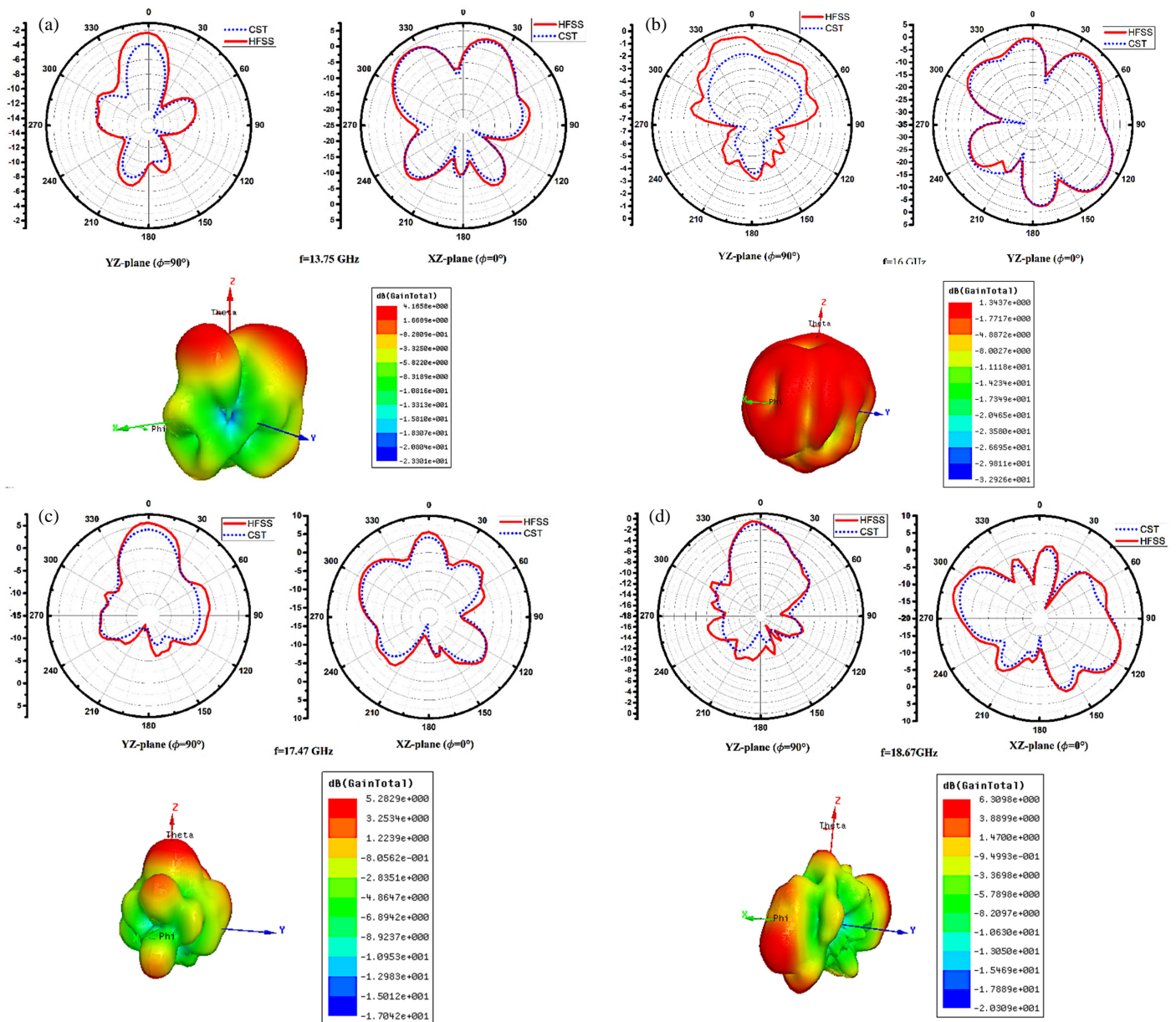

FIGURE 22. 2D and 3D gain radiation patterns at the four resonant frequencies: (a) 13.75 GHz, (b) 16 GHz, (c) 17.47 GHz, and (d) 18.67 GHz.
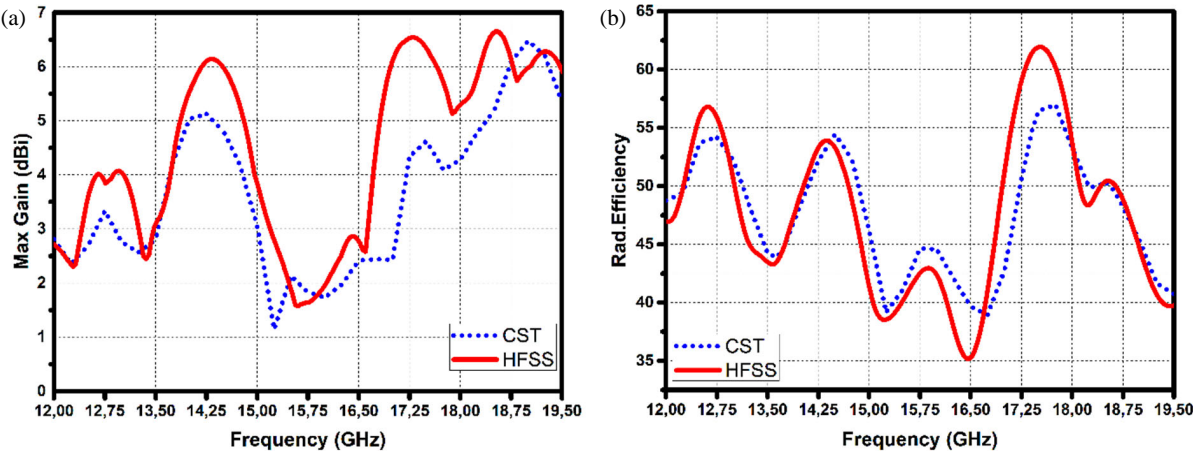
FIGURE 23. Comparison of (a) simulated gain and (b) radiation efficiency by CST and HFSS.

TABLE 2. Comparison of proposed wideband antenna and some earlier published work.

References / Properties	Proposed work	[14]	[20]	[17]	[21]	[23]	[13]	[24]	[22]	[19]	[18]	[8]
Year	-	2024	2023	2023	2022	2022	2020	2020	2020	2019	2018	2018
Frequency Band	Ku	Ku	X	Ku	Ku	X	Ku	X	X	C	Ku	Ku
FBW (%)	41	19.96	13	14.63 13.30	4.91	15.92	4.4 24.29	12.8	22.4	11.9	5.7	13.53
Max Gain (dBi)	6.6	8.98	9.224	6.68	6.05	5.71	6.82	7.1	6.45	4.3	6,4	4
Substrate Material	Epoxy FR-4	Epoxy FR-4	Rogers RT Duroid 5880	Rogers RT Duroid 5880	Epoxy FR-4	Rogers RT Duroid 5880	Epoxy FR-4	Rogers RT Duroid 5880	Rogers RT Duroid 5880	F4B-2	TLY0 31	Rogers RT Duroid 5880
Size substrate (L×W×h) (mm³)	29.7× 22× 1.6	30 × 30 × 1.6	40 × 34 × 1.575	31.85× 28× 1.57	38× 35× 1.5	17.1× 15× 1.57	42× 42× 1.6	30× 24.9× 1.6	29.5× 23.5× 1.57	41,8× 41,8× 1.57	20× 20× 0.787	32.7× 15.4× 1.57

characteristic. Figure 23(b) shows that the radiation efficiency results from CST and HFSS simulations are in good agreement, with the HFSS simulation indicating a higher efficiency range of 35% to 62%. Although the antenna offers several advantages, a notable drawback is the use of low-cost FR4 material as the substrate, which leads to unstable gain and lower efficiency values due to higher losses at higher frequencies.

To emphasize the significance of this proposed research, Table 2 presents a comparison of various parameters between the suggested design and earlier published designs. It can be observed that our antenna achieves the widest fractional bandwidth among the reported works. In addition to improved bandwidth, the suggested antenna is fabricated on the most affordable substrate material, resulting in the most economical production cost while maintaining moderate gain. Furthermore, it is more compact than most of the antennas discussed in the literature.

4. CONCLUSION

A wideband, low-cost, cavity-backed slotted antenna utilizing SIW technology is designed and analyzed in this article. The proposed antenna incorporates bilateral slots and a modified ground plane and is fabricated on an affordable FR4 substrate with dimensions of $29.7 \times 22 \times 1.6\,\text{mm}^3$. A parametric study was conducted to achieve wideband performance. The measured impedance bandwidth of the antenna is 6.68 GHz (12.82–19.5 GHz), covering nearly the entire Ku-band, with a fractional bandwidth of 41%. Additionally, the simulated results indicate that the antenna offers diverse radiation patterns and a maximum gain of approximately 6.6 dBi, making it a strong candidate for satellite applications. Another notable advantage of the proposed antenna is its low production cost and compact size compared to previous designs.

REFERENCES

[1] Deslandes, D. and K. Wu, "Integrated microstrip and rectangular waveguide in planar form," *IEEE Microwave and Wireless Components Letters*, Vol. 11, No. 2, 68–70, 2001.

[2] Xu, F. and K. Wu, "Guided-wave and leakage characteristics of substrate integrated waveguide," *IEEE Transactions on Microwave Theory and Techniques*, Vol. 53, No. 1, 66–73, 2005.

[3] Yan, X. and M. Guo, "Broadband cross-coupled filter based on CPW structure and triangular SIW resonant cavity," *Progress In Electromagnetics Research Letters*, Vol. 120, 59–64, 2024.

[4] Abdullah Al-Gburi, A. J., "5G MIMO antenna: Compact design at 28/38 GHz with metamaterial and SAR analysis for mobile phones," *Przeglad Elektrotechniczny*, Vol. 2024, No. 4, 171–174, 2024.

[5] Luo, G. Q., Z. F. Hu, L. X. Dong, and L. L. Sun, "Planar slot antenna backed by substrate integrated waveguide cavity," *IEEE Antennas and Wireless Propagation Letters*, Vol. 7, 236–239, 2008.

[6] Yun, S., D.-Y. Kim, and S. Nam, "Bandwidth enhancement of cavity-backed slot antenna using a via-hole above the slot," *IEEE Antennas and Wireless Propagation Letters*, Vol. 11, 1092–1095, 2012.

[7] Sievenpiper, D., H.-P. Hsu, and R. M. Riley, "Low-profile cavity-backed crossed-slot antenna with a single-probe feed designed for 2.34-GHz satellite radio applications," *IEEE Transactions on Antennas and Propagation*, Vol. 52, No. 3, 873–879, 2004.

[8] Heydarzadeh, F. and M. H. Neshati, "Design and development a wideband SIW based cavity-backed slot antenna using two symmetrical circular corner perturbations," *International Journal of RF and Microwave Computer-Aided Engineering*, Vol. 28, No. 9, e21552, 2018.

[9] Yun, S., D.-Y. Kim, and S. Nam, "Bandwidth and efficiency enhancement of cavity-backed slot antenna using a substrate removal," *IEEE Antennas and Wireless Propagation Letters*, Vol. 11, 1458–1461, 2012.

[10] Ali, H. A., E. Massoni, L. Silvestri, M. Bozzi, L. Perregrini, and A. Gharsallah, "Increasing the bandwidth of cavity-backed SIW antennas by using stacked cavities," *International Journal of Microwave and Wireless Technologies*, Vol. 10, No. 8, 942–947, 2018.

[11] Mukherjee, S., A. Biswas, and K. V. Srivastava, "Broadband substrate integrated waveguide cavity-backed bow-tie slot antenna," *IEEE Antennas and Wireless Propagation Letters*, Vol. 13, 1152–1155, 2014.

[12] Kumar, A. and S. Raghavan, "Broadband SIW cavity-backed triangular-ring-slotted antenna for Ku-band applications," *AEU — International Journal of Electronics and Communications*, Vol. 87, 60–64, 2018.

[13] Hadi, R. M., M. Y. Yousif, and F. M. Ali, "Design of SIW wideband curved slot antenna for radar and satellite applications," Vol. 62, No. 4, 10, 2020.

[14] Chrij, D., A. Khabba, J. Amadid, Z. E. Ouadi, S. Ibnyaich, and A. Zeroual, "Bandwidth of SIW cavity-backed antenna by using square-shaped slot for Ku band applications," in *2024 International Conference on Global Aeronautical Engineering and Satellite Technology (GAST)*, 1–6, Marrakesh, Morocco, 2024.

[15] Farashahi, M., E. Zareian-Jahromi, and R. Basiri, "A compact semi-open wideband SIW horn antenna for K/Ku band applications," *AEU — International Journal of Electronics and Communications*, Vol. 92, 15–20, 2018.

[16] Nakmouche, M. F., D. E. Fawzy, A. M. M. A. Allam, H. Taher, and M. F. A. Sree, "Dual band SIW patch antenna based on H-slotted DGS for Ku band application," in *2020 7th International Conference on Electrical and Electronics Engineering (ICEEE)*, 194–197, Antalya, Turkey, 2020.

[17] Patil, S. M. and R. Venkatesan, "Bandwidth enhancement of substrate integrated waveguide cavity-backed half bow-tie complementary-ring slot antenna for Ku-band applications," *Alexandria Engineering Journal*, Vol. 81, 46–54, 2023.

[18] Heydarzadeh, F. and M. H. Neshati, "Design and development a wideband SIW based cavity-backed slot antenna using two symmetrical circular corner perturbations," *International Journal of RF and Microwave Computer-Aided Engineering*, Vol. 28, No. 9, e21552, 2018.

[19] Niu, B. and J.-H. Tan, "Bandwidth enhancement of low-profile SIW cavity antenna with bilateral slots," *Progress In Electromagnetics Research Letters*, Vol. 82, 25–32, 2019.

[20] Paliwal, G. J., A. Kumar, and J. Sengupta, "SIW cavity-backed slot antenna using high-order radiation modes for broadband applications in X band," in *2023 IEEE International Symposium On Antennas And Propagation (ISAP)*, 1–2, Kuala Lumpur, Malaysia, 2023.

[21] Ali, F., "Low profile Substrate Integrated Waveguide (SIW) wideband antenna for Ku-band Applications," in *Proceedings of 2nd International Multi-Disciplinary Conference Theme: Integrated Sciences and Technologies, IMDC-IST 2021*, Sakarya, Turkey, 2022.

[22] Bollavathi, L., V. Dorai, and S. Alapati, "Wideband planar substrate integrated waveguide cavity-backed amended dumbbell-shaped slot antenna," *AEU — International Journal of Electronics and Communications*, Vol. 127, 153489, 2020.

[23] Althuwayb, A. A., D. Chaturvedi, and A. Kumar, "Substrate integrated waveguide (SIW) cavity-backed slot antenna with monopole-like radiation for vehicular communications," *Applied Physics A*, Vol. 128, No. 3, 202, 2022.

[24] Lokeshwar, B., D. Venkatasekhar, and A. Sudhakar, "Bandwidth-enhanced of SIW cavity-backed slot antenna by perturbing TE_{210} cavity mode," *Bioscience Biotechnology Research Communications*, Vol. 13, No. 14, 320–324, 2020.